

Momentum shearing interferometry of electron waves

Thierry Ruchon^a, Thomas Remetter^a, Per Johnsson^{a,*}, Johan Mauritsson^a, Erik Gustafsson^a, Marko Swoboda^a and Anne L'Huillier^a

^aDepartment of Physics, Lund University, P. O. Box 118, 221 00 Lund, Sweden

ABSTRACT

We analyse recent experiments on momentum shearing interferometry of electron wave packets^{1,2} by using an optical analogy with shearing interferometry for optical waves. This analogy offers a convenient point of view to discuss the capabilities and difficulties of this technique used to access the phase of electron wave packets.

Keywords: attosecond technology, shearing interferometry.

1. INTRODUCTION

The retrieval of the phase of a wave in optics relies on the transfer of the phase information into intensity information. Two general techniques have been used to achieve this goal: either one splits the wave in small parts using a gate, and measure the phase of each part, or one mixes the wave with a reference – which may be itself, and retrieve the phase information from the interferences between the two waves. The former technique includes the Shack-Hartmann interferometer, which uses an array of micro-lenses as a spatial gate to get the spatial phase of a wave front, and the FROG-like techniques, which use a temporal gate to get the temporal phase of a pulse. The latter includes the shearing interferometry devices, which use two spatially shifted replica of the same wave front to get a spatial phase, and the SPIDER-like techniques which use two spectrally shifted replica to get a temporal phase. Due to the development of adaptive optics and ultra short pulsed lasers, these techniques have received considerable attention in the past years. Great developments in the speed and quality of the computational methods have followed. Interestingly, the SPIDER-like techniques have now been extended to electron wave-packets: the RABITT technique, which is used to characterize the spectral phase of an electronic pulse of attosecond duration coming in a train, may be seen as a degenerated SPIDER³ and a direct transposition of SPIDER to the measurement of isolated attosecond pulses was proposed by Quéré *et al.*⁴. It has been shown recently that the phase of the wave front of an attosecond electronic pulse could also be measured to some extent by a shearing technique^{1,2}. With regards to the work done in the optical domain, it seems desirable to have an analogy, as accurate as possible, between this electronic interferometer and the optical spatial shearing interferometer. Not only this might make it possible to take advantage of the computational capabilities developed for the optical versions, but it could trigger some new experimental developments as well. In this proceeding we build such an analogy.

The proceeding is organized as follows. In section 2 we review the principle of spatial shearing interferometry for electronic pulses. Section 3 is dedicated to the description of an optical shearing interferometer that follows closely the electronic one. We eventually discuss some images simulated for this interferometer and conclude.

2. MOMENTUM SHEARING INTERFEROMETRY OF ELECTRON WAVE PACKETS

The experimental scheme of momentum shearing interferometry of electron wave packets^{1,2} follows the general principles of shearing interferometry, that is i) create two identical replica of the wave front to be characterized, then ii) shift one with respect to the other, and iii) make them interfere. Step one is achieved by photoionizing a noble gas by successive attosecond XUV pulses in the sensitive region of a Velocity Map Imaging Spectrometer (VMIS)^{5,6}. Attosecond *electronic* pulses are created. Since the source of attosecond pulses of XUV light delivers

Further author information: (Send correspondence to T. Ruchon)

T. Ruchon: E-mail: thierry.ruchon@fysik.lth.se, Telephone: +46 46 222 3832

* Currently at FOM-Institute AMOLF, Kruislaan 407, 1098 SJ Amsterdam, The Netherlands.

trains of XUV pulses, the electronic pulses come as trains as well. Every other attosecond electronic pulse is then shifted upwards while the other is shifted downwards in momentum space by a probe IR field, which is just opposite for two successive attosecond electronic pulses (fig. 1.b). This constitutes the second step. For the third step, the wave packets are recombined on a MCP (Micro Channel Plate) and interfere (fig. 1.c). The train of attosecond pulses might be decomposed in couples of successive oppositely shifted pulses which all interfere. One difference with respect to the traditional shearing scheme is that in the electronic version, a Fabry-Perot effect due to the repetition of the process is superimposed, as apparent in figure 1. Fourier analysing the region of overlap of the electrons distributions, one can – partly – retrieve the phase of the electronic wave front.

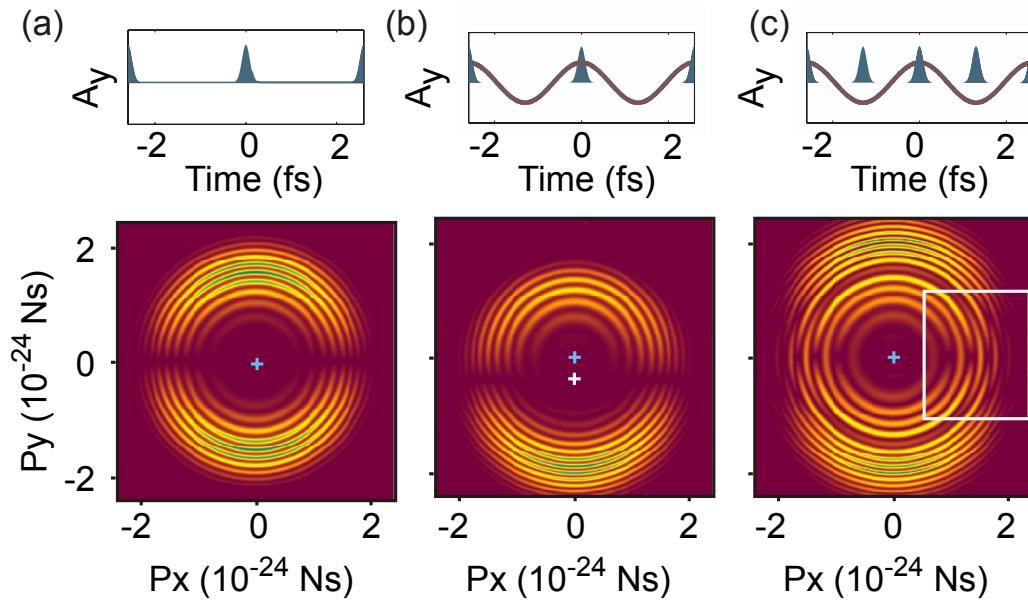


Figure 1. Principle of momentum shearing interferometry of electron wave packets. (a) Ionization by a series of attosecond pulses gives the photoionization pattern of the species modulated by a ring pattern. (b) Photoionization in the presence of an IR field with maximum vector potential shifts the distribution opposite to the direction of the vector potential. The interference rings remain centered on the same location. (c) Ionization by successive attosecond pulses separated by half the period of the IR field shifts the distributions in opposite directions, giving an extra interference pattern (white box). The figures presented are calculated with the strong field approximation procedure in the case of helium using trains of 4 pulses.

The attosecond source at Lund Laser Center was used for demonstration experiments of this technique. It delivers attosecond pulse trains shaped by spectral and spatial filtering of high harmonic generation (HHG) in argon^{7,8} or in neon⁹, with 170 as (resp. 130 as) duration and 30 eV (resp. 80 eV) central frequency. The repetition rate of the attosecond pulses is either 1.3 fs, that is half the period of the IR field used for HHG, or 2.7 fs, that is the period of the IR field¹⁰. The attosecond pulse train is inserted in a Mach-Zehnder interferometer which allows for its superposition with part of the IR beam used for its generation with a precisely controlled delay. Photo-ionization can be monitored using either a Magnetic Bottle Electron Spectrometer (MBES) or a VMIS. To implement the shearing interferometry scheme, the argon source, with two pulses per cycle was used, in combination with the VMIS.

Using Strong Field Approximation calculations¹¹ and assuming infinitely short pulses, one may get the following expression for the electron distribution in momentum space in the shearing configuration¹:

$$I(\vec{p}) = |a_{\vec{p}}|^2 \propto \left| \sum_k (-1)^k |d_y[\vec{p} + (-1)^k \cdot \vec{p}_s]| e^{-i\varphi_a(\vec{p} + (-1)^k \cdot \vec{p}_s)} \cdot e^{-i\Phi(kT/2)} \right|^2. \quad (1)$$

In this equation $I(\vec{p})$ is the probability distribution of the electrons, where \vec{p} is the coordinate in momentum

space; $a_{\vec{p}}$ is the amplitude distribution; d_y is the complex one photon dipole matrix element in the direction of the XUV field and φ_d its phase, which is to be characterized; $\vec{p}_s = e\vec{A}_0$ is the shear, where \vec{A}_0 is the amplitude of the vector potential of the IR field; T is its period; e is the charge of the electron and \hbar the reduced Planck constant. The summation is carried out over all pulses in the train. The phase term, $\Phi(kT/2)$ originates from the quasi-classical action describing the motion of an electron ionized at time $kT/2$ in the IR field and is given by $\Phi(kT/2) = ((p_x^2 + p_y^2)/2m\hbar + I_p + U_p) \cdot kT/2$, where I_p denotes the ionization energy and U_p the ponderomotive energy ($U_p = e^2 A_0^2/4m$).

To gain some insight into this equation, we first consider only two consecutive pulses. Equation 1 then writes

$$I(\vec{p}) \propto |d_y(\vec{p}+\vec{p}_s)|^2 + |d_y(\vec{p}-\vec{p}_s)|^2 + 2 \cdot |d_y(\vec{p}+\vec{p}_s)| \cdot |(d_y(\vec{p}-\vec{p}_s))| \cdot \cos\left(\frac{p^2}{2m\hbar} \cdot T/2 + \varphi_d(\vec{p}+\vec{p}_s) - \varphi_d(\vec{p}-\vec{p}_s) + \phi_0\right) \quad (2)$$

where ϕ_0 is a phase depending only on A_0^2 . This is the equation giving the intensity distribution for a usual two-wave interferometer in optics. Indeed it describes the interference of two shifted replica of the same wave. The shift between the two waves, \vec{p}_s , is adjustable via the amplitude of the vector potential. Due to the quadratic variation of the cosine term with \vec{p} , a high frequency circular fringe pattern shows up. Its periodicity does not depend on \vec{A}_0 . The location of the bright fringes, for a given \vec{A}_0 , depend only on the relative phase $\varphi_d(\vec{p}+\vec{p}_s) - \varphi_d(\vec{p}-\vec{p}_s)$. Measuring their location thus gives access to the relative phase between two parts of the electronic wave packet. The experimental proof of principle of the scheme was described in ref. 1.

Now, taking into account all pulses, one sees on equation 1 that this is equivalent to coherently sum up the 2-pulses interference patterns with increasing delays by steps of T . Like in a Fabry Perot interferometer, as the number of couple of pulses increases, the fringes will get narrower.

3. OPTICAL ANALOG TO THE ELECTRONIC INTERFEROMETER

In an attempt to get an analogy between the electronic and optical versions of the shearing interferometers, equation 2 will be used as a guide. The interference pattern essentially consists of rings. As a consequence, it seems natural to take as a starting point a Michelson interferometer which has its mirrors perpendicular one to the other. Such a device is schematized in figure 2.a. The equivalent unfolded scheme is given in figure 2.b. It is illuminated by a monochromatic point source located in S . The source might be followed by an amplitude and phase mask (Mk). The assembly, source plus mask, is hereafter called the source, whose wave front is to be measured. We consider a point M on a screen. The electric field emitted by the source, may be written as a function of the direction of propagation given by the unit vector $\vec{u} = \vec{SM}/|\vec{SM}|$ as

$$E_0(\vec{u}) = f(\vec{u}) \cdot e^{i \cdot \phi(\vec{u})} \cdot e^{i \cdot (\vec{k} \cdot \vec{r} - \omega \cdot t)}. \quad (3)$$

In this equation, the real function $f(\vec{u})$ gives the radiation pattern of the source. For instance, for the fundamental mode of a laser it would be a Gaussian function. $\phi(\vec{u})$ is the phase function which should be retrieved, \vec{k} is the wave vector given by $\vec{k} = \frac{2\pi}{\lambda} \cdot \vec{u}$, where λ is the wavelength, $\vec{r} = \vec{SM}$, ω is the pulsation of the light and t stands for time. The difference in path length between the two arms is denoted δ .

Letting this source propagate through the Michelson interferometer is equivalent to creating two sources, labeled S_1 and S_2 , which are located on the z -axis at $-d - \delta/2$ and $-d + \delta/2$, respectively, where d is the mean distance from S_1 and S_2 to the screen (Fig 2.b). The electric field in M is now the sum of the electric fields emitted by the two sources:

$$E(\vec{M}) = f_1(\vec{u}_1) \cdot e^{i \cdot \phi_1(\vec{u}_1)} \cdot e^{i \cdot (\vec{k}_1 \cdot \vec{r}_1 - \omega \cdot t)} + f_2(\vec{u}_2) \cdot e^{i \cdot \phi_2(\vec{u}_2)} \cdot e^{i \cdot (\vec{k}_2 \cdot \vec{r}_2 - \omega \cdot t)}. \quad (4)$$

The intensity then reads

$$I(M) = |f_1(\vec{u}_1)|^2 + |f_2(\vec{u}_2)|^2 + 2 \cdot |f_1(\vec{u}_1)| \cdot |f_2(\vec{u}_2)| \cdot \cos(\phi_1(\vec{u}_1) - \phi_2(\vec{u}_2) + \vec{k}_1 \cdot \vec{r}_1 - \vec{k}_2 \cdot \vec{r}_2). \quad (5)$$

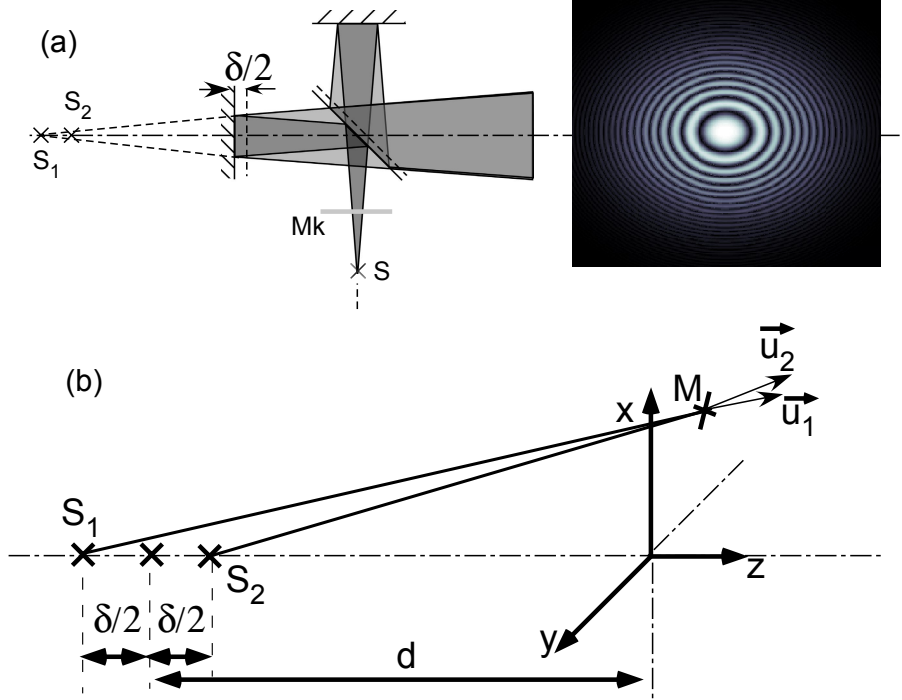


Figure 2. (a). Principle of a Michelson interferometer. The two mirrors are orthogonal. To simplify the discussion, the compensator is omitted. The optical path difference between the two arms is δ . It is illuminated by a divergent source coming from the bottom, followed by an amplitude and phase mask (Mk). The picture to the right is a simulated interference pattern with a source having uniform intensities and no extra phase from the mask. (b) Equivalent scheme to (a).

We use a coordinate system so that M is located in $(x, y, 0)$ (see Fig 2.b). Considering $d \gg \delta$, the phase in the cosine of Eq. (5) becomes

$$\vec{k}_1 \cdot \vec{r}_1 - \vec{k}_2 \cdot \vec{r}_2 \simeq \frac{2\pi\delta}{\lambda} - \frac{\pi \cdot \delta}{\lambda} \cdot \frac{x^2 + y^2}{d^2} \quad (6)$$

Equation (5) then reads

$$I(M) = |f_1(\vec{u}_1)|^2 + |f_2(\vec{u}_2)|^2 + 2 \cdot |f_1(\vec{u}_1)| \cdot |f_2(\vec{u}_2)| \cdot \cos\left(\frac{\pi \cdot \delta}{\lambda} \cdot \frac{x^2 + y^2}{d^2} - \phi_1(\vec{u}_1) + \phi_2(\vec{u}_2) - \frac{2\pi\delta}{\lambda}\right). \quad (7)$$

Equations (5) and (2) are very similar. Nevertheless, with this setup, since \vec{u}_1 and \vec{u}_2 are very close one another (fig. 2.b), the shear is extremely small. Moreover, it cannot be adjusted while keeping the fringe spacing constant, that is δ . To correct this defect in the analogy, the scheme is now slightly modified to get the one depicted in figure 3^{12,13}. First, the plate used as a beam splitter is replaced by a thin wedge with angle $\delta\theta$. It results in opposite rotations of the mean directions of propagation of both beams by an angle close to $\delta\theta$ (basic calculations leading to this result are presented in the appendix). This constitutes an adjustable shear. The mean directions of propagation are respectively denoted $\vec{u}_1^{(0)}$ and $\vec{u}_2^{(0)}$. Second, the beams in each arm are shifted laterally by delay stages consisting of two mirrors, so that the virtual sources still lie on the z -axis and are still separated by the delay δ . Now, the electric fields of the two virtual sources write:

$$E_1(\vec{u}) = E_0(\vec{u} - \vec{u}_1^{(0)}) = f(\vec{u} - \vec{u}_1^{(0)}) \cdot e^{i \cdot \phi(\vec{u} - \vec{u}_1^{(0)})} \quad (8)$$

$$E_2(\vec{u}) = E_0(\vec{u} - \vec{u}_2^{(0)}) = f(\vec{u} - \vec{u}_2^{(0)}) \cdot e^{i \cdot \phi(\vec{u} - \vec{u}_2^{(0)})}. \quad (9)$$

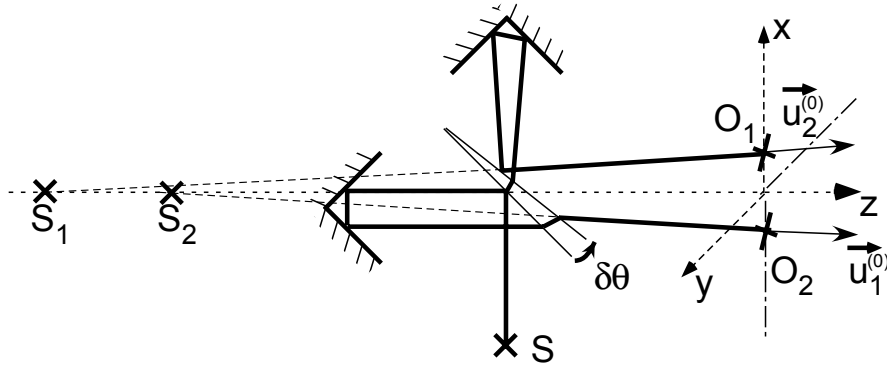


Figure 3. Modified Michelson interferometer. A wedge is used as a beam splitter and corner cubes as retro-reflectors to laterally shift the virtual sources S_1 and S_2 . It results in an adjustable mean direction of propagation of the beams, i.e. an adjustable spatial shear not linked to the delay. Now the central parts of the two sources hit the screen in O_1 and O_2 .

Equation (5) becomes

$$I(M) = |f(\vec{u}_1 - \vec{u}_1^{(0)})|^2 + |f(\vec{u}_2 - \vec{u}_2^{(0)})|^2 + 2 \cdot |f(\vec{u}_1 - \vec{u}_1^{(0)})| \cdot |f(\vec{u}_2 - \vec{u}_2^{(0)})| \cdot \cos\left(\frac{\pi \cdot \delta}{\lambda} \cdot \frac{x^2 + y^2}{d^2} - \phi(\vec{u}_1 - \vec{u}_1^{(0)}) + \phi(\vec{u}_2 - \vec{u}_2^{(0)}) - \frac{2\pi\delta}{\lambda}\right), \quad (10)$$

Equations (2) and (10) now show exactly the same features.

Eventually, to obtain equation (1), the interference pattern should be repeated several times. To get the optical analog, we consider a number of partially transparent plates in each arm instead of simple mirrors (fig. 4). Their transmittance is adjusted so that all outgoing beams have the same amplitude. Moreover, the distance between two successive plates in each arm should be equal to twice the distance imbalance between the arms. This arrangement gives back equation (1). Table 1 sums up the correspondences between the two types of interferometers progressively described in this section.

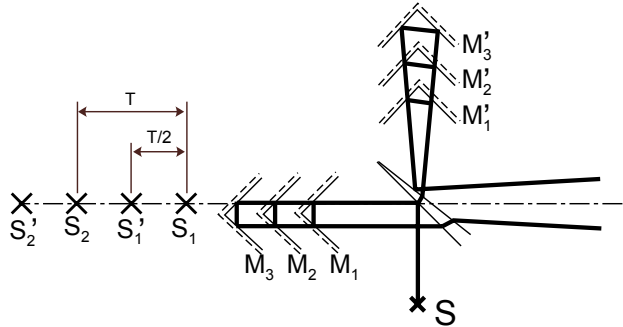


Figure 4. Michelson-Fabry-Perot type interferometer equivalent to the electronic shearing interferometer. The successive semi-reflective corners in each arm are spaced by twice the distance imbalance between the arms.

4. COMPUTATIONS AND DISCUSSIONS

In this section, some interferograms computed using the interferometers depicted in fig. 3 and in fig. 4 are successively discussed.

	Electron Interferometer	Optical interferometer
Space	Momentum space	Usual space
Shear	Amplitude of the vector potential of the IR field	Angle of the wedge
Modulation	Repetition rate of the pulses	Optical path difference
Airy function	Number of pulses in the train	Number of retro-reflectors

Table 1. Correspondence of the different parameters between the optical and the electronic interferometers.

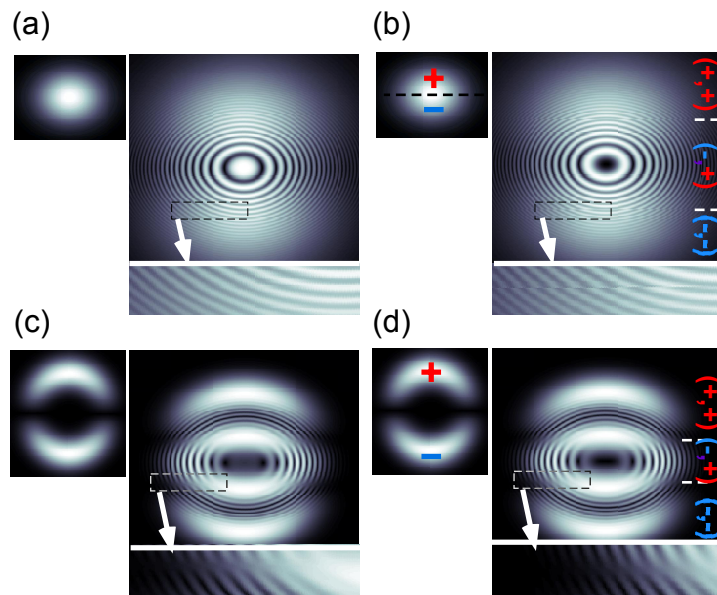


Figure 5. Interferograms simulated for the interferometer depicted in figure 3. (a) and (b) Gaussian source with (a) flat phase front and (b) π phase jump in the middle of the field. (c) and (d) “p-wave like” source with (c) both lobes having the same signs, (d) lobes of opposite signs.

In the case of the two beams interferometer of fig. 3, we first used a gaussian distribution of intensity as a source (fig. 5 (a) and (b)). As expected, the light accumulates in the two off axis directions $\vec{u}_1^{(0)}$ and $\vec{u}_2^{(0)}$ due to the two first terms in the right hand side of equation (10). The separation between the two spots can be adjusted tuning the angle of the wedge. It is modulated by an interference pattern which appears as fringes centered on the z-axis. This is controlled by the delay balance between the two arms. Any phase difference in between the different parts of the beam is encoded in this interference pattern. For instance, when the phase front has a constant phase, the fringes are continuous (fig. 5.a), whereas when there is a π phase jump in the middle of the front, this shows up as two discontinuities in the rings, located in the middle of the two spots (fig. 5.b). Besides, it should be noted that there are no fringes in the upper and lower parts of the field, where the beams do not overlap.

We also computed the interferograms for a p-wave. The results are reported in figure 5.c, for a constant phase over the wave front, and in figure 5.d for a wave front with a π phase jump between the two lobes. The general pattern is the sum of the two oppositely shifted p-waves, modulated by some rings centered on the z-axis. One can clearly identify the phase jump as discontinuities in the fringe pattern, located on the node where they smear out in figure 5.d. It intuitively shows that on the one hand, if one wants to be able to identify a phase jump, the shear should be adjusted so that the interferences cover all three zones as in figure 5. On the other hand, if one wants to measure the phase with a high resolution within one lobe, the shear should be small. Practically then, in the electronic case, it is necessary to have a convenient way of adjusting the shear to fully reconstruct the phase.

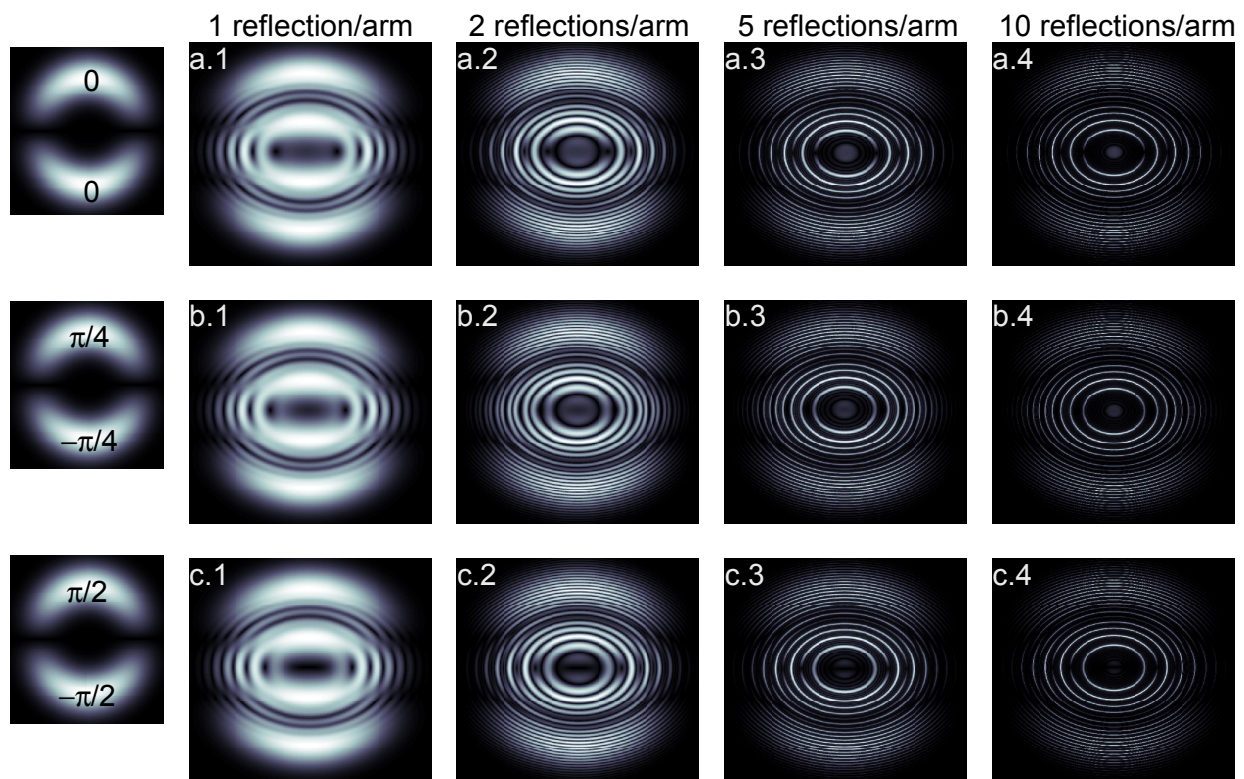


Figure 6. Interferograms simulated for the interferometer depicted in figure 4 with a “p-wave like” source. First line: same phase for the two lobes, and successively 1 (a.1), 2 (a.2), 5 (a.3), and 10 (a.4) pairs of mirrors. Line (b): $\pi/2$ shift between the two lobes, same numbers of mirrors. Line (c): π shift between the two lobes, same numbers of mirrors.

We now turn to the case of the interferometer schematized in figure 4. Figure 6 reports some simulations in the case of a p-wave source, with either no phase shift a $\pi/2$ or a π phase shift between the two lobes. The

number of pairs of mirrors is increased from 1 in figs. (a) to 2 (figs. (b)), 5 (figs. (c)) and 10 pairs (figs. (d)). Going from column 1 to column 2, one sees a double frequency appearing, as expected from the double delay in between the successive mirrors in each arm compared to the arm imbalance (fig. 4). In addition, some fringes, having this double frequency, are now obtained in the upper and lower parts of the field, where light coming from the multiple reflections in each of the two arms interfere together. Fig. 1 was calculated for 4 pulses. It compares well to the second column of fig. 6.

As the number of reflexions increases, the Fabry Perot Airy function builds up, yielding thinner and thinner fringes. The third column uses 5 pairs of mirrors, which corresponds approximately to the number of pulses we have in our train of attosecond pulses. It seems clear from figure 6 that even with a higher number of reflexions and such thin fringes, a π phase shift remains accessible. The progressive contrast inversion going from figure 6 (a.4) to fig. 6 (c.4) can clearly be identified. Nevertheless it is identified only by intensity variations at one single location in the field for the fringes are very thin. The detection of such a phase shift then entirely relies on both the high density of channels on the detector, on the dynamics of this detector and on the noise/statistics of the electrons counts. Indeed, Fourier transforming the data might not be the best one since the modulation is no longer sinusoidal: the modulation peak spreads out, making the use of the usual filtering procedure of the SPIDER algorithm difficult. Consequently, it does not seem recommended to use too long pulse trains for momentum shearing interferometry in momentum space.

5. CONCLUSION

We have proposed an optical equivalent to momentum shearing of electron wave packets. The simplicity of the calculations in the optical case makes the tool convenient to investigate the requirements and limits of the technique. We have shown that, if the resolution of the image is not a problem and the dynamics range of the detector high enough, even a rather long train of pulses can give information on the phase of the electron wave packet. Now, if these are too poor, the use of short trains should be preferred. Nevertheless, such a trade-off should also include the usual low number of XUV photons in the short trains compared to the long ones, which then favors long trains. Our analogy may also be used to derive a systematic computational procedure to retrieve the phase of electron wave packets using an arbitrary long train. To the best of our knowledge, the adaptation of the SPIDER procedure to an Airy modulation instead of a sinusoidal one has not been carried out so far. This may give a more convenient way to use the images of the electronic shearing interferometer.

APPENDIX A. CALCULATION OF THE COORDINATES OF THE VIRTUAL SOURCES OF THE SHEARING INTERFEROMETER

In this appendix the deviations are calculated for the two beams of the interferometer depicted in figure 3. θ_0 denotes the angle of the wedge and n its refractive index. Following the notations given in figure 7.a and making use of Snell-Descartes relations, the following equalities hold for the the beam transmitted on the first interface:

$$\theta_2 = \arcsin\left(\frac{\sin \theta_1}{n}\right) \quad (11)$$

$$\theta_3 = \theta_2 - \theta_0 \quad (12)$$

$$\theta_4 = \arcsin(n \cdot \sin \theta_3) \quad (13)$$

$$\theta_5 = \theta_4 + \theta_0 - \frac{\pi}{4} \quad (14)$$

$$\theta_6 = \frac{\pi}{4} - \theta_5 - \theta_0 \quad (15)$$

$$\delta\theta_2 = \frac{\pi}{4} + \theta_0 - \theta_6 \quad (16)$$

Combining these equations, one gets the following expression for the deviation:

$$\delta\theta_2 = -\frac{\pi}{4} + 3 \cdot \theta_0 + \arcsin \left[n \cdot \sin \left(\arcsin\left(\frac{\sin \theta_1}{n}\right) - \theta_0 \right) \right] \quad (17)$$

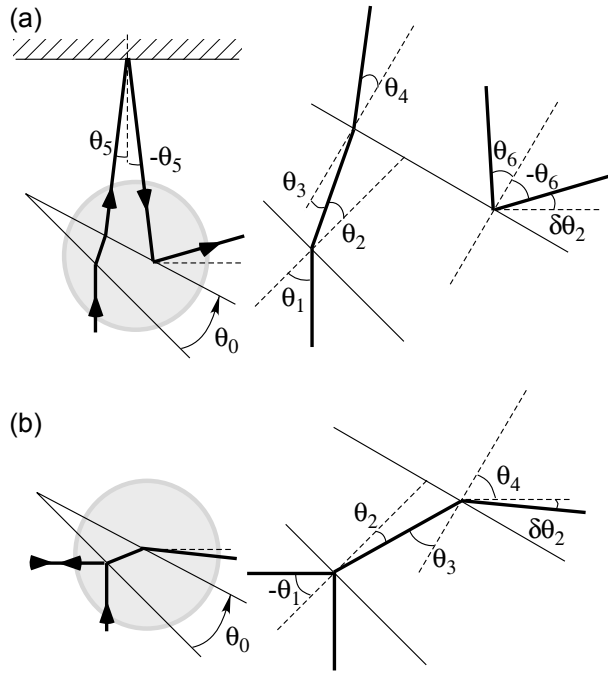


Figure 7. Definition of the angles for the calculation of the deviation. All angles are oriented from the dashed line to the continuous line.

In the case of the beam reflected on the first interface, we have the relations:

$$\theta_2 = \arcsin\left(\frac{\sin -\theta_1}{n}\right) \quad (18)$$

$$\theta_3 = \theta_2 - \theta_0 \quad (19)$$

$$\theta_4 = \arcsin(n \cdot \sin \theta_3) \quad (20)$$

$$\delta\theta_1 = \frac{\pi}{4} + \theta_0 + \theta_4 \quad (21)$$

Combining them, one gets

$$\delta\theta_1 = \frac{\pi}{4} + \theta_0 + \arcsin\left[n \cdot \sin\left(\arcsin\left(\frac{\sin -\theta_1}{n}\right) - \theta_0\right)\right] \quad (22)$$

One can directly see that in the limit $n=1$, the deviation $\delta\theta_1$ vanishes whereas $\delta\theta_2$ goes to $2\theta_0$, in agreement with physical expectations. For more realistic cases, computations show that the deviations are just in opposite directions.

ACKNOWLEDGMENTS

This research was supported by the Integrated Initiative of Infrastructure LASERLAB-EUROPE (RII3-CT-2003-506350) within the 6th European Community Framework Programme, the Marie Curie Research Training Network XTRA (MRTN-CT-2003-505138), The Marie Curie Intra-European Fellowships (MEIF-CT-2006-040577), the Swedish Science Council and the Knut and Alice Wallenberg Foundation.

References

- [1] T. Remetter, P. Johnsson, J. Mauritsson, K. Varjú, Y. Ni, F. Lépine, E. Gustafsson, M. Kling, J. Khan, R. López-Martens, K. J. Schafer, M. J. J. Vrakking, and A. L'Huillier, "Attosecond Electron Wave Packet Interferometry," *Nature Phys.* **2**, p. 323, 2006.
- [2] K. Varjú, P. Johnsson, J. Mauritsson, T. Remetter, T. and Ruchon, Y. Ni, F. Lépine, M. Kling, J. Khan, K. J. Schafer, M. J. J. Vrakking, and A. L'Huillier, "Angularly resolved electron wave packet interferences," *Journal of Physics B: Atomic, Molecular and Optical Physics* **39**(18), pp. 3983–3991, 2006.
- [3] H. G. Muller, "Reconstruction of attosecond harmonic beating by interference of two-photon transitions," *Appl. Phys. B* **74**, p. 17, 2002.
- [4] F. Quéré, J. Itatani, G. L. Yudin, and P. B. Corkum, "Attosecond Spectral Shearing Interferometry," *Phys. Rev. Lett.* **90**, p. 073902, 2003.
- [5] R. Dorner, V. Mergel, O. Jagutzki, L. Spielberger, J. Ullrich, R. Moshammer, and H. Schmidt-Bocking, "Cold Target Recoil Ion Momentum Spectroscopy: a 'momentum microscope' to view atomic collision dynamics," *Physics Reports* **330**, pp. 95–192, 2000.
- [6] A. T. J. B. Eppink and D. H. Parker, "Velocity map imaging of ions and electrons using electrostatic lenses: Application in photoelectron and photofragment ion imaging of molecular oxygen," *Rev. Sci. Instrum.* **68**, p. 3477, 1997.
- [7] R. López-Martens, K. Varjú, P. Johnsson, J. Mauritsson, Y. Mairesse, P. Salières, M. B. Gaarde, K. J. Schafer, A. Persson, S. Svanberg, C.-G. Wahlström, and A. L'Huillier, "Amplitude and Phase Control of Attosecond Light Pulses," *Phys. Rev. Lett.* **94**, p. 033001, 2005.
- [8] P. Johnsson, R. López-Martens, S. Kazamias, J. Mauritsson, C. Valentin, T. Remetter, K. Varjú, M. B. Gaarde, Y. Mairesse, H. Wabnitz, P. Salières, P. Balcou, K. J. Schafer, and A. L'Huillier, "Attosecond Electron Wave Packet Dynamics in Strong Laser Fields," *Phys. Rev. Lett.* **95**, p. 013001, 2005.
- [9] E. Gustafsson, T. Ruchon, M. Swoboda, R. L. Martens, P. Balcou, and A. L'huillier, "Broadband attosecond pulse shaping," *Optics Letters* , 2007. submitted.
- [10] J. Mauritsson, P. Johnsson, E. Gustafsson, A. L'Huillier, K. J. Schafer, and M. B. Gaarde, "Attosecond Pulse Trains Generated Using Two Color Laser Fields," *Phys. Rev. Lett.* **97**, p. 013001, 2006.
- [11] M. Lewenstein, P. Balcou, M. Ivanov, A. L'Huillier, and P. B. Corkum, "Theory of high-order harmonic generation by low-frequency laser fields," *Phys. Rev. A* **49**, p. 2117, 1994.
- [12] G. S. Sarkisov, "Shearing inteferometer with an air wedge for the electron density diagnostics in a dense plasma.," *Instruments and experimental techniques* **39**, pp. 727–731, 1996.
- [13] S. A. Pikuz, V. M. Romanova, N. V. Baryshnikov, M. Hu, B. R. Kusse, D. B. Sinars, T. A. Shelkovenko, and D. A. Hammer, "A simple air wedge shearing interferometer for studying exploding wires," *Papers from the thirteenth topical conference on high temperature plasma diagnostics* **72**(1), pp. 1098–1100, AIP, 2001.